An ultra-short polarization beam splitter based on dual-core photonic crystal fiber with surface plasmon resonance effect

Ke Wang,[a,1] Yuwei Qu,[a,1] Jinhui Yuan,[a,b,*] Shi Qiu,[a] Xian Zhou,[b] Binbin Yan,[a] Qiang Wu,[c,d,*] Bin Liu,[d] Kuiru Wang,[a] Xinzhu Sang,[a] Chongxiu Yu[a]

[a]State Key Laboratory of Information Photonics and Optical Communications, Beijing University of Posts and Telecommunications, Beijing 100876, China
[b]Research Center for Convergence Networks and Ubiquitous Services, University of Science & Technology Beijing (USTB), Beijing 100083, China
[c]Department of Physics and Electrical Engineering, Northumbria University, Newcastle upon Tyne, NE1 8ST, United Kingdom
[d]Key Laboratory of Nondestructive Test (Ministry of Education), Nanchang Hangkong University, Nanchang 330063, China

Abstract. In this paper, an ultra-short polarization beam splitter (PBS) based on dual-core photonic crystal fiber (DC-PCF) with surface plasmon resonance (SPR) effect is proposed. The finite element method is used to investigate the coupling characteristics between the core mode and surface plasmon polariton (SPP) mode. The influences of the PCF structure parameters on the coupling length (*CL*) and coupling length ratio (*CLR*) are also investigated. The normalized output powers of the x-polarization and y-polarization are calculated, and the optimized PBS achieves an ultra-short length of 62.5 μm. The splitting bandwidth of 110 nm (1.51~1.61 μm) is achieved when the extinction ratio (*ER*) is less than - 20 dB. The minimum *ER* reaches -71 dB at the wavelength of 1.55 μm. The proposed PBS has an important application in the high-speed optical communication system.

Keywords: polarization beam splitter, photonic crystal fiber, surface plasmon resonance, extinction ratio.

[1]These authors contributed equally to this work.
*yuanjinhui81@bupt.edu.cn; qiang.wu@northumbria.ac.uk

1. Introduction

With the rapid development of the communication system, the polarization characteristics of optics have attracted great attention. Because the polarization beam splitter (PBS) can split a beam of light into two polarized beams 1, it has widespread applications in optical communication and sensing systems. The larger refractive index difference between the two polarization beams is the key to achieve the PBS with shorter length and wider bandwidth. However, it is difficult to obtain the larger refractive index difference for the traditional dual-core optical fibers because of their structural symmetry and low birefringence 2. Compared with the traditional optical fibers, photonic crystal fiber (PCF) has unique optical characteristics, such as endlessly single-mode 5,6, high birefringence 7, large mode field area 10, controllable dispersion 11, and high nonlinearity 12. Thus, the PCF can be applied for different devices. For example, the PCF-based PBS with shorter length and wider bandwidth could be -achieved.

In recent years, some researchers designed different kinds of PBS based on the dual-core PCF (DC-PCF) through breaking the structural symmetry of the DC-PCF, which can be achieved by changing the arrangement of the air holes in the cladding region 19 or introducing the elliptical air holes 19. Moreover, other materials can also be used for replacing the silica substrate and the metal materials can be used for coating or filling the air holes. In 2015, Xu *et al*. reported a DC-PCF PBS with an elliptical hole, which is filled with a kind of low refractive index material. The length and bandwidth of the reported PBS are 401 μm and 140 nm 22. In

2016, Wang *et al.* designed a DC-PCF PBS filled with the liquid crystal in the air hole, achieving the PBS length of 890.5 μm and bandwidth of 150 nm 23. In 2017, Wang *et al*. proposed a DC-PCF PBS with the magnetic fluid added in the air hole, where the PBS length and bandwidth are 5.1 mm and 189 nm 24. In 2018, Wang *et al*. reported a rectangular-hexagonal structure DC-PCF PBS with two elliptical holes in the core region, along with the PBS length of 93.3 μm and bandwidth of 40 nm 25. In 2019, Xu *et al*. demonstrated a DC-PCF PBS filled with titanium and low refractive index liquid, where the PBS length and bandwidth are 83.9 μm and 32.1 nm 26. In 2020, Qu *et al*. investigated a gold-coated silicon DC-PCF PBS, where the PBS length and mid-infrared bandwidth are 192 μm and 830 nm 27.

In this paper, we propose an ultra-short PBS based on the gold-filled DC-PCF. The two cores of the DC-PCF are composed by the three elliptical air holes in the horizontal axis. Two elliptical gold wires are filled in longitudinal axis to induce the surface plasmon resonance (SPR) effect. The PBS can achieve an ultra-short length of 62.5 μm and a bandwidth of 110 nm. The proposed DC-PCF PBS has an important application in the high-speed optical communication system.

2. Design of the DC-PCF PBS and theory

The cross-section of the proposed DC-PCF PBS is shown in Fig. 1. The diameter of all circular air holes arranged in the triangular array is d, and the hole-to-hole pitch is Λ_1. In addition, the three layers of air holes are arranged in a rectangular array in the horizontal direction, and the hole-to-hole pitch is Λ_2. The air hole in the most center is replaced with an elliptical hole, whose minor and major axes are denoted by d_{x1} and d_{y1}, respectively. And the two air holes are missing on the left and right sides of the central elliptical air hole to form the cores A and B, respectively. The air holes on the upper and lower sides of the central elliptical hole are filled by the two elliptical gold wires, whose minor and major axes are denoted by d_{y2} and d_{x2}, respectively. Compared with other metal materials, the gold material has stable chemical property, good biomolecular compatibility, and strong corrosion resistance. The left side of the core A and right side of the core B are replaced by the two large elliptical air holes, whose minor and major axes are denoted by d_{x3} and d_{y3}, respectively.

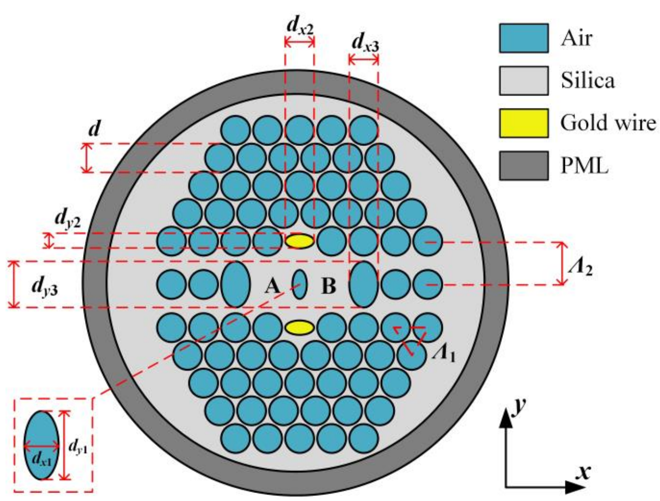

Fig. 1. The cross-section of the proposed DC-PCF PBS.

The background material is the pure silica. The perfect matching layer (PML) of the proposed DC-PCF is set at the outermost layer to absorb the radiation energy 28. The inner diameter and thickness of the PML are 6 μm and 1.2 μm, respectively. The material of the PML is highly doped silica, and the corresponding refractive index is n_{silica}+0.03. The material dispersions of the silica and doped silica can be described by the Sellmeier equation [29, 30]. The dielectric constant of the gold material can be described by the Drude-Lorentz 31

$$\varepsilon_m = \varepsilon_\infty - \frac{\omega_D^2}{\omega\left(\omega + j\gamma D\right)} - \frac{\Delta\varepsilon \cdot \Omega_L^2}{\left(\omega^2 - \Omega_L^2\right) - j\Gamma_L \omega}, \tag{1}$$

where ε_m represents the dielectric constant of gold, ε_∞ = 5.9673 is the high frequency dielectric constant, Δ_ε = 1.09 is the wave vector, ω is the angular frequency of the light, and ω_D and γ_D are the plasma frequency and Damping frequency, respectively. Here, $\omega_D/2\pi$ = 2113.6 THz, and $\gamma_D/2\pi$ = 15.92 THz. Ω_L and Γ_L are the frequency and spectral width of the Lorentz oscillation, respectively. $\Omega_L/2\pi$ = 650.07 THz, and $\Gamma_L/2\pi$ = 104.86 THz.

The coupling length (*CL*) of the DC-PCF, where the light power is completely transferred from one core to the other one, can be calculated by 32

$$CL_{x,y} = \frac{\lambda}{2\left(n_{x,y}^{even} - n_{x,y}^{odd}\right)}, \tag{2}$$

where the $CL_{x,y}$ is the *CL* of the *x*-pol and *y*-pol, λ is the wavelength of the incident light, and n is the effective refractive indices of the even and odd modes. In order to achieve the complete beam splitting, the *CL* of the two polarization states needs to satisfy the condition that $mCL_x = nCL_y = L$ (m and n are the positive integers and L is the length of the PBS), and the coupling length ratio (*CLR*) can be calculated by

$$CLR = \frac{CL_y}{CL_x}, \tag{3}$$

When the *CLR* reaches 2 or 0.5, the splitting length is the optimum value. The transmission loss of the ultra-short PBS is also negligible. Therefore, when the input power P_{in} is determined, the normalized output power P_{out} can be calculated by 33

$$P_{out}^{x,y} = P_{in}^{x,y} \cos^2\left(\frac{\pi L}{2CL_{x,y}}\right), \tag{4}$$

The performance of the PBS can be described by the extinction ratio (*ER*) as following 34

$$ER = 10 \cdot \lg\left(\frac{p_{out}^{y}}{p_{out}^{x}}\right), \tag{5}$$

when the *ER* is larger than 20 dB, the propagated light could be completely split, so the *ER* can determine the bandwidth of the PBS.

3. Simulation results and discussion

The finite element method (FEM) is adopted to simulate the proposed DC-PCF PBS. Fig. 2 shows the calculated effective refractive indices of the *x*-pol odd and even modes, *y*-pol odd and even modes, *x*-pol and *y*-pol first SPP modes, and zero SPP mode. From Fig. 2, the *x*-pol even mode and *x*-pol first SPP mode have a resonance point at wavelength 1.17 μm, the *y*-pol odd mode and *y*-pol first SPP mode have a resonance point at wavelength 1.22 μm, and the *y*-pol even mode and zero SPP mode have a resonance point at wavelength 1.3 μm, while there is no resonance point between the *x*-pol odd mode and SPP mode. According to the coupling mode theory 35, the *x*-pol even, *y*-pol odd, and *y*-pol even modes are completely coupled with the *x*-pol first SPP, *y*-pol first SPP, and zero SPP modes, respectively. In order to further verify the above conclusions, the mode field distributions of the *x*-pol and *y*-pol even and odd modes at wavelengths 1.05 μm and 1.55 μm are shown in Figs. 3(a) and 3(b), respectively. From Fig. 3(a), the mode field energies of the *x*-pol and *y*-pol odd and even modes do not occur to change at wavelength 1.05 μm, which indicate that before wavelength 1.05 μm, there are no mode coupling between the considered modes and SPP modes. From Fig. 3(b), the mode field energy of the *x*-pol odd mode does not occur to change, and the mode field energies of the *x*-pol even, *y*-pol odd, and *y*-pol even modes occur to transfer. It indicates that the *x*-pol even, *y*-pol odd, and *y*-pol even modes occur to couple with the *x*-pol first SPP mode, *y*-pol first SPP mode, and zero SPP mode, respectively, after 1.55 μm. Because the coupling strengths based on the SPR effect for different modes are different, the effective refractive index differences between the *x*-pol and *y*-pol modes are increased, and the DC-PCF PBS could be achieved due to the enhanced birefringence.

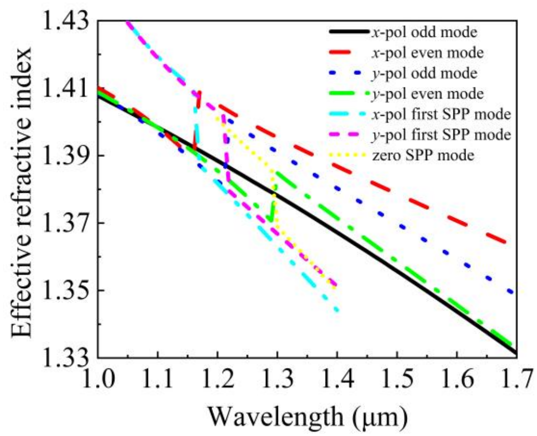

Fig. 2. The effective refractive indices of the *x*-pol odd and even modes, *y*-pol odd and even modes, *x*-pol and *y*-pol first SPP modes, and zero SPP mode calculated as functions of wavelength.

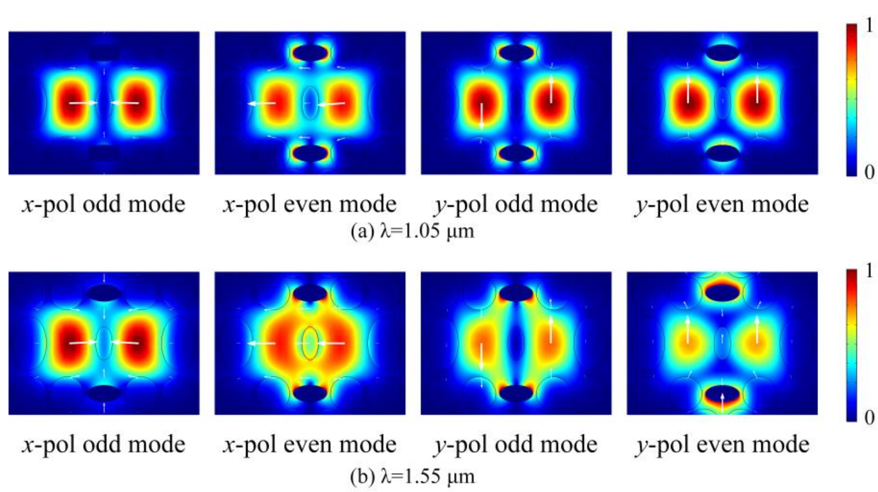

Fig. 3. The mode field distributions of the *x*-pol odd mode, *x*-pol even mode, *y*-pol odd mode, and *y*-pol even mode calculated at wavelengths (a) 1.05 μm and (b) 1.55 μm.

In the following, the structure parameters, including d, Λ_1, Λ_2, d_{x1}, d_{y1}, d_{y2}, d_{x2}, d_{x3}, and d_{y3}, are, respectively, adjusted at wavelength 1.55 μm to optimize the performance of the DC-PCF PBS. The relationships between the CL_x, CL_y, and CLR and d are shown in Fig. 4. When d changes from 0.95 to 1.05 μm, the effective refractive indices of the x-pol odd and even modes decrease, but the decrease amplitude of the x-pol even mode is larger than that of the x-pol odd mode. Meanwhile, the effective refractive indices of the y-pol odd and even modes also decrease, but the decrease amplitude of the y-pol even mode is larger than that of the y-pol odd mode. Thus, the effective refractive index differences between the x-pol odd and even modes and y-pol odd and even modes become smaller. As shown in Fig. 4, the CL_x increases from 28 to 33 μm, and the CL_y decreases from 92 to 52 μm. It can be deduced from Eq. (3) that the CLR decreases from 3.2 to 1.5 μm. When d=1 μm, the CLR=2.048, which is very close to the ideal value of 2.

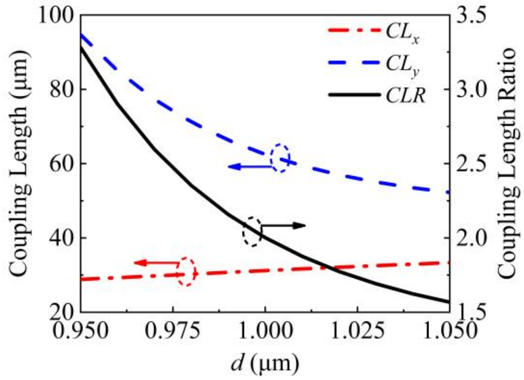

Fig. 4. The relationships between the CL_x, CL_y, and CLR and d.

When Λ_1 changes from 1.05 to 1.15 μm, the effective refractive indices of the x-pol odd and even modes increase, and the increase amplitude of the x-pol even mode is approximately equal to that of the x-pol odd mode. Although the effective refractive indices of the y-pol odd and even modes also increase, the increase amplitude of the y-pol even mode is larger than that of the y-pol odd mode. Thus, the effective refractive index difference between the x-pol odd and even modes remains almost unchanged, while the effective refractive index difference between the y-pol odd and even modes becomes smaller. As shown in Fig. 5(a), the CL_x is stabilized at 30 μm, and the CL_y increases from 43 to 120 μm. According to Eq. (3), the CLR increases from 1.4 to 3.8 μm. When Λ_1=1.11 μm, the CLR is very close to 2. From Fig. 5(b), when Λ_2 changes from 1.4 to 1.7 μm, the CL_x increases from 29 to 33 μm, the CL_y increases from 52 to 109 μm, and the corresponding CLR increases from 1.79 to 3.2. When Λ_2=1.6 μm, the CLR is very close to 2.

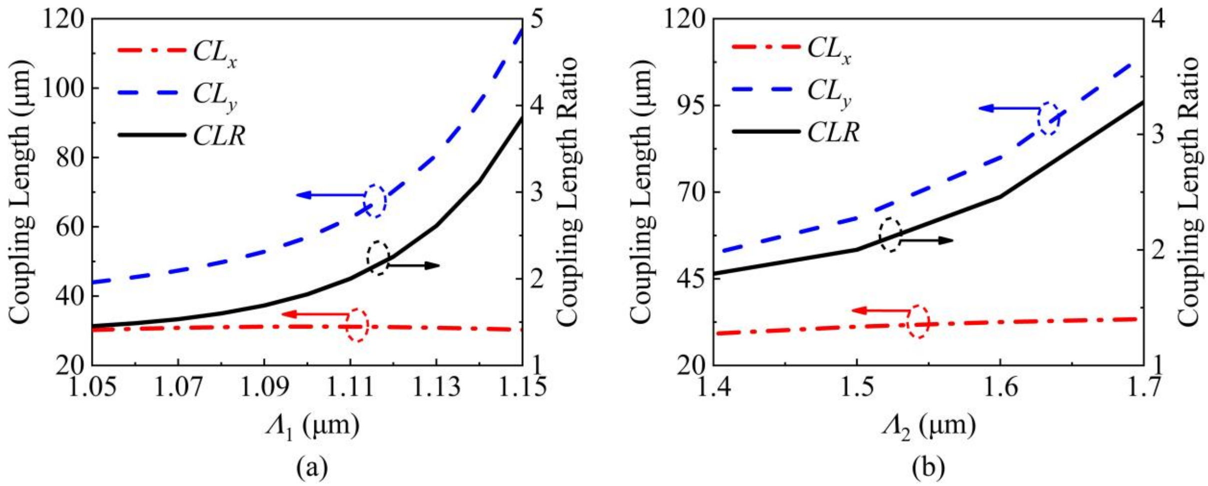

Fig. 5. The relationships between the CL_x, CL_y, and CLR and (a) Λ_1 and (b) Λ_2.

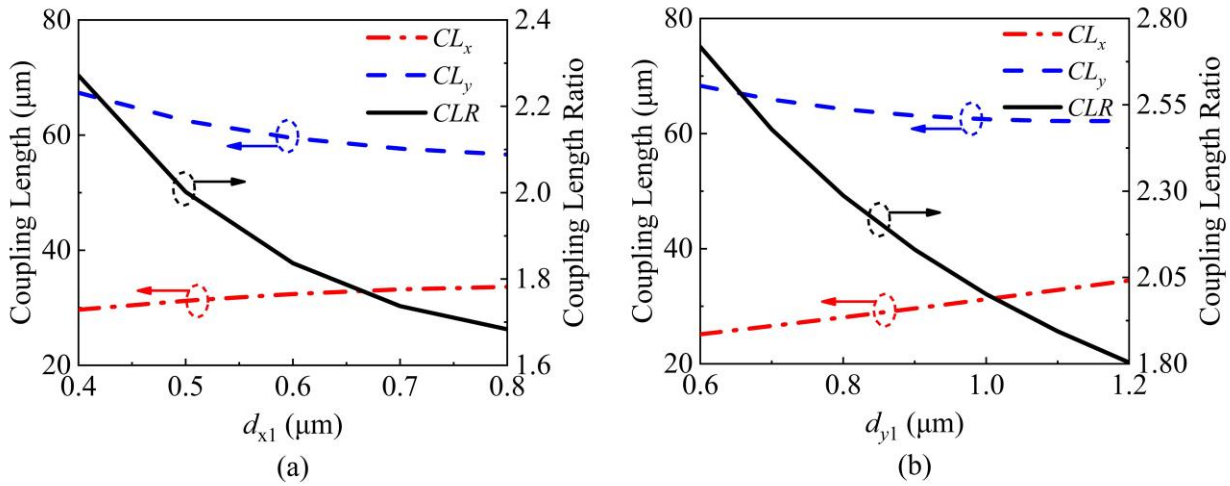

Fig. 6. The relationships between the CL_x, CL_y, and CLR and (a) d_{x1} and (b) d_{y1}.

The influences of the elliptical hole sizes are shown in Figs. 6(a) and 6(b). When d_{x1} changes from 0.4 to 0.8 μm, the effective refractive indices of the *x*-pol odd and even modes decrease, but the decrease amplitude of the *x*-even mode is larger than that of the *x*-odd mode. Although the effective refractive index of the *y*-pol odd mode remains almost unchanged, the effective refractive index of the *y*-pol even mode gradually decreases. Thus, the effective refractive index difference between the *x*-pol odd and even modes becomes smaller, and the effective refractive index difference between the *y*-pol odd and even modes becomes larger. As shown in Fig. 6(a), the CL_x increases from 29 to 33 μm, the CL_y decreases from 67 to 56 μm, and the corresponding *CLR* decreases from 2.2 to 1.6. When d_{x1}=0.5 μm, the *CLR* is very close to 2. When d_{y1} increases from 0.6 to 1.2, the effective refractive index difference of the *x*-pol odd and even modes becomes smaller, and the effective refractive index difference between the *y*-pol odd and even modes also becomes larger. As shown in Fig. 6(b), the CL_x increases from 25 to 34 μm, the CL_y decreases from 68 to 62 μm, and the corresponding *CLR* decreases from 2.7 to 1.8. When d_{y1}=1 μm, the *CLR* is very close to 2.

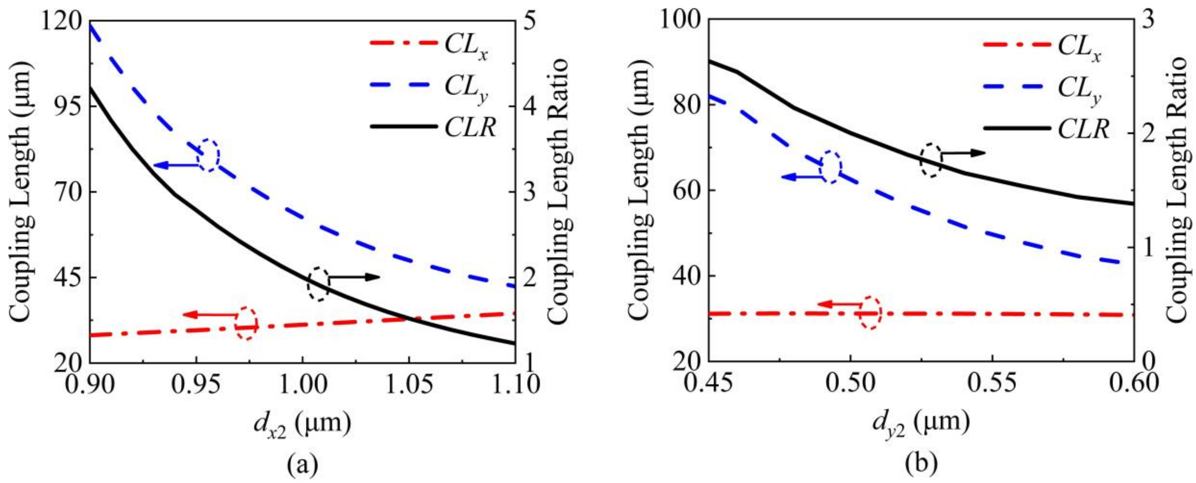

Fig. 7. The relationships between the CL_x CL_y, and CLR and (a) d_{x2} and (b) d_{y2}.

The influences of the elliptical gold wires are shown in Figs. 7(a) and 7(b). When d_{x2} changes from 0.9 to 1.1 μm, the effective refractive index of the x-pol odd mode remains almost unchanged, but the effective refractive index of the x-pol even mode gradually decreases. Although the effective refractive indices of the y-pol odd and y-pol even modes decrease, the decrease amplitude of the y-pol even mode is larger than that of the y-pol odd mode. Thus, the effective refractive index difference between the x-pol odd and x-pol even modes becomes smaller, and the effective refractive index difference between the y-pol odd and y-pol even modes becomes larger. As shown in Fig. 7(a), the CL_x increases from 28 to 34 μm, the CL_y decreases from 118 to 42 μm, and the corresponding CLR decreases from 4.2 to 1.2. When d_{x2}=1 μm, the CLR=2. When d_{y2} increases from 0.45 to 0.6, the effective refractive index difference between the x-pol odd and x-pol even modes remains almost unchanged, and the effective refractive index difference between the y-pol odd and y-pol even modes becomes larger. As shown in Fig. 7(b), the CL_x is stabilized s at 30 μm, the CL_y decreases from 131 to 42 μm, and the corresponding CLR decreases from 4.2 to 1.38. When d_{y2}=0.5 μm, the CLR is very close to 2.

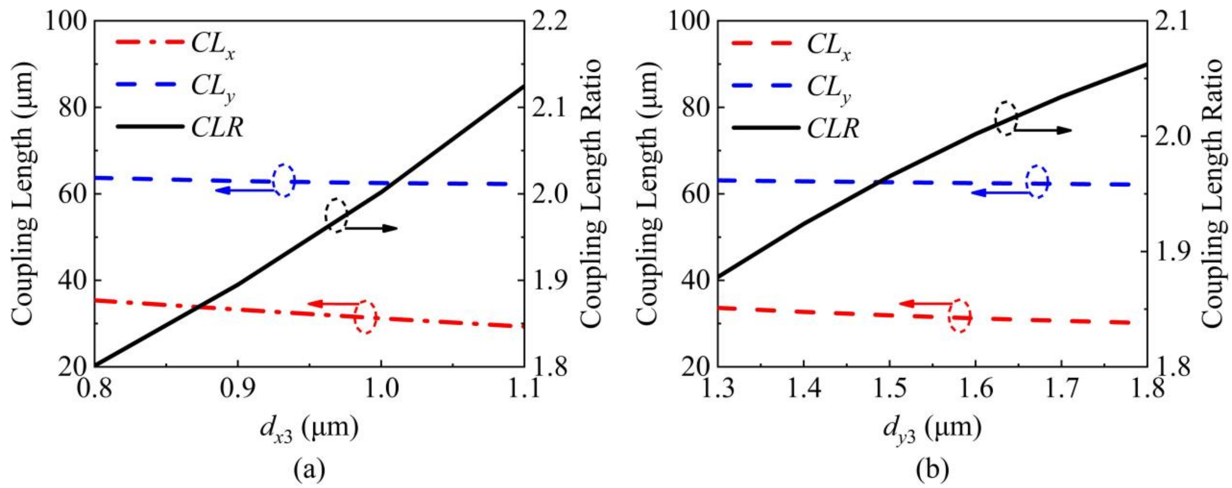

Fig. 8. The relationships between the CL_x CL_y, and CLR and (a) d_{x3} and (b) d_{y3}.

The influences of the large elliptical air hole along the horizontal axis are shown in Figs. 8(a) and 8(b). When d_{x3} changes from 0.8 to 1.1 μm, the effective refractive index of the x-pol odd mode decreases slightly, and the effective refractive index of the *x*-pol even mode remains almost unchanged. Meanwhile, the effective refractive indices of the *y*-pol odd and *y*-pol even modes remain almost unchanged. Thus, the effective refractive index difference between the *x*-pol odd and *x*-pol even modes becomes larger, and the effective refractive index differences between the *y*-pol odd and *y*-pol even modes changes slightly. From Fig. 8(a), as the CL_x decreases, the CL_y is almost constant, and the corresponding *CLR* increases. As d_{y3} increases from 1.3 to 1.8, the effective refractive indices of the *x*-pol odd and *x*-pol even modes and *y*-pol odd and *y*-pol even modes decrease, and the decrease amplitudes of the *x*-pol odd and *y*-pol odd modes are approximately equal to those of the *x*-pol even and *y*-pol even modes. It can be seen from Fig. 8(b) that the CL_x and CL_y are almost constant, but the corresponding *CLR* increases.

As shown in Fig. 9(a), when the gold wire is not filled in the two elliptical air holes, the *CLR* can only maintain at 1.1 in the wavelength range from 1.4 to 1.7 μm. At this time, it is difficult to completely split the polarized light between the two cores. As shown in Fig. 9(b), when the two elliptical air holes are filled with the gold wires, the *CLR* decreases from 2.21 to 1.98 in the considered wavelength range, and reaches 2 at wavelength 1.55 μm. Therefore, the gold wire plays an important role in achieving the PBS.

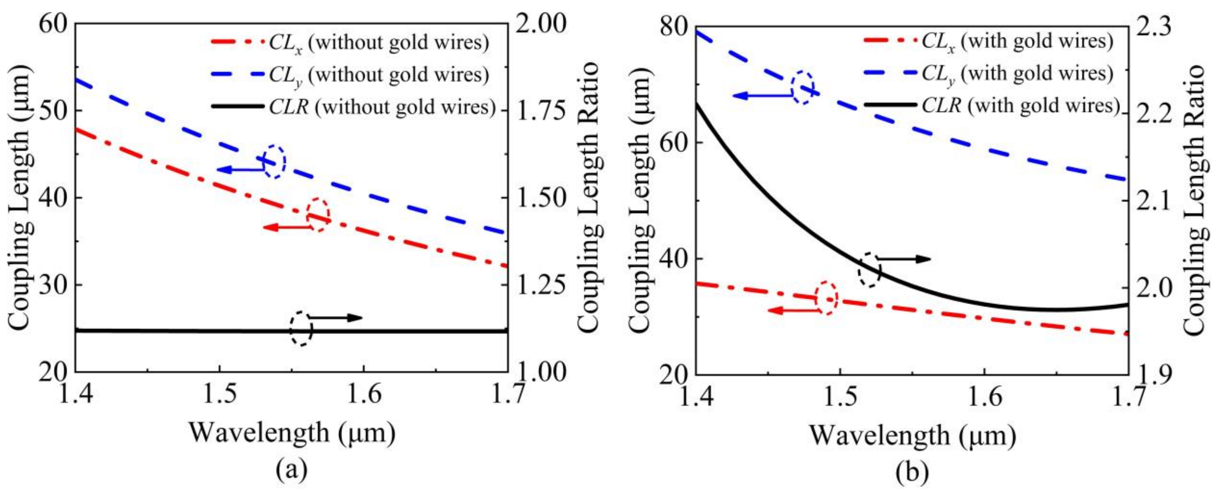

Fig. 9. The relationships between the *CL* and *CLR* and wavelength, (a) without gold wires, and (b) with gold wires.

In summary, the optimized structure parameters of the DC-PCF PBS are chosen as following: Λ_1=1.11 μm, Λ_2=1.5 μm, *d*=1 μm, d_{x1}=0.5 μm, d_{y1}=1 μm, d_{x2}=1 μm, d_{y2}=0.5 μm, d_{x3}=1 μm, and d_{y3}=1.6 μm. Fig. 10(a) shows the relationship between P_{out} of *x*-pol and *y*-pol and propagation distance. As shown in Fig. 10(a), when the light at wavelength 1.55 μm enters the core A, P_{out} of the *x*-pol and *y*-pol will periodically change with the propagation distance. When the propagation distance is 62.5 μm, P_{out} of the *x*-pol reaches the maximum value, and P_{out} of the *y*-pol is close to 0. At this time, the two polarization states can be completely separated. For the core B, the case is exactly opposite. Due to the ohmic loss of metal, the maximum value of the normalized power will decrease with the propagation distance 36. Thus, the optimal DC-PCF PBS length is 62.5 μm. Fig. 10(b) shows the relationship between the *ER* and wavelength when the DC-PCF PBS length is 62.5 μm. It can be seen from Fig. 10(b) that the *ER* reaches the maximum value of -71 dB at wavelength 1.55 μm, and is less than -20 dB in the wavelength range of 1.5 to 1.61 μm. The bandwidth of the DC-PCF PBS is 110 nm, covering the whole C band.

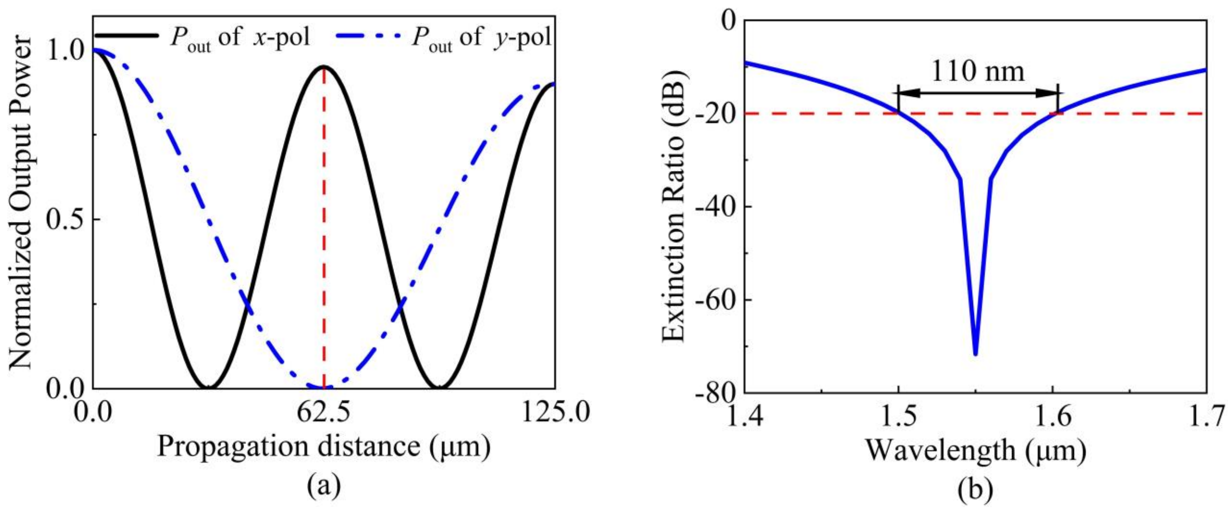

Fig. 10. (a) The relationship between P_{out} of the x-pol and y-pol and propagation distance, and (b) the relationship between the *ER* and wavelength.

Table 1. The comparisons between other proposed PCF PBSs and this work.

Reference	PBS length	Bandwidth	*ER* at 1550 nm
22	1.890 mm	9 nm	-83.2 dB
23	0.175 mm	250 nm	-80.7 dB
25	1.0 mm	280 nm	-83.6 dB
26	1.746 mm	47 nm	-60 dB
Error! Reference source not found.	830 μm	20 nm	-60 dB
[42]	254.6 μm	560 nm	-111 dB
This work	62.5 μm	110 nm	-71 dB

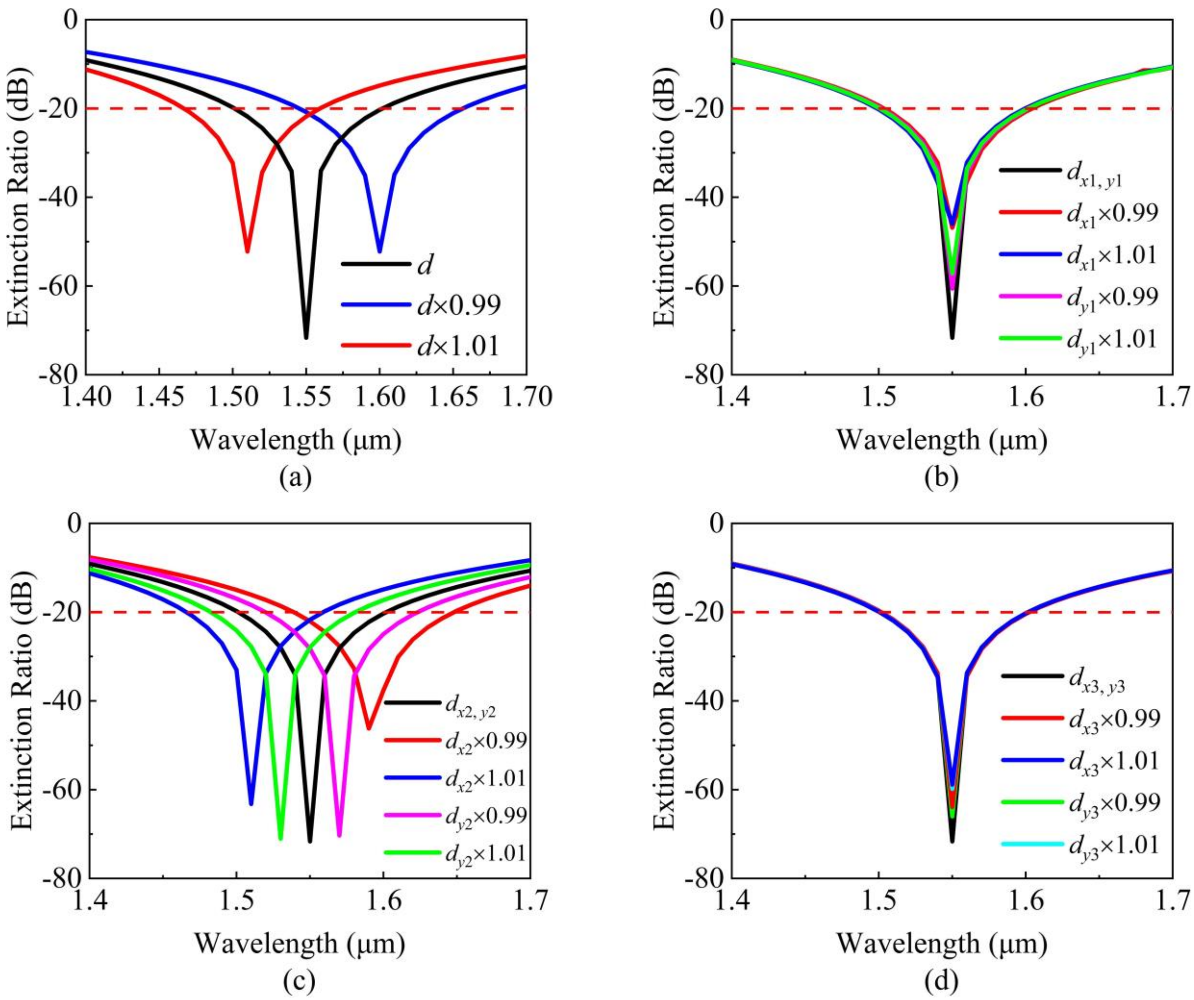

Fig. 11. The relationships between the *ER* and wavelength under ±1% error of (a) d, (b) d_{x1}, d_{y1} (c) d_{x2}, d_{y2}, and (d) d_{x3}, d_{y3}.

Table 1 shows the comparisons between other proposed PCF PBSs and this work [37-42]. It can be concluded from Table 1 that although the bandwidths of the PBSs proposed in Refs [38, 39, 42] are slightly wider than that of this work, the DC-PCF PBS proposed in this work has the shortest length. This is more conducive to the development of photonic integration. Moreover, the bandwidth and *ER* are also good. Finally, we will consider the fabrication tolerance of the proposed DC-PCF PBS. We investigated the dependence of the *ER* on each structure parameter under the fabrication tolerance of 1%. As shown in Fig. 11(a), when d is reduced or increased by 1%, the bandwidth is red-shifted to 1.54 - 1.64 μm or blue-shifted to 1.46 - 1.56 μm. The DC-PCF PBS can still work well. As shown in Figs. 11(b) and 11(d), when d_{x1} and d_{y1}, and d_{x3} and d_{y3} are reduced or increased by 1%, only the *ER* at wavelength 1.55 μm is changed, and the bandwidth of the proposed DC-PCF PBS does not change. As shown in Fig. 11(c). when d_{x2} and d_{y2} are reduced by 1%, the bandwidth is blue-shifted to 1.53 - 1.65 μm and 1.51 - 1.63 μm, respectively. When d_{x2} and d_{y2} are increased by 1%, the bandwidth is red-shifted to 1.43- 1.57 μm and 1.41- 1.57 μm, respectively. Therefore, the proposed DC-PCF PBS has good fabrication tolerance.

4. Conclusion

In conclusion, we design an ultra-short DC-PCF PBS based on the SPR effect. The performance of the proposed DC-PCF PBS is optimized through adjusting structure parameters. The *CLR* at wavelength 1.55 μm is very close to 2. The optimized DC-PCF PBS length is 62.5 μm, the *ER* at wavelength 1.55 μm is -68.76 dB, and the bandwidth is 110 nm (1.5 - 1.61 μm), which can cover the whole C band. The proposed DC-PCF PBS has ultra-short length, large bandwidth, and high *ER*, and can find important application in the micro-optical system.

Disclosures

The authors declare no conflicts of interest.

Acknowledgement

This work is supported by National Key Research and Development Project of China (2019YFB2204001).

References

1.W. L. Lu, S. Q. Lou, X. Wang, et al. "Ultrabroadband polarization splitter based on three-core photonic crystal fibers," *Appl. Opt.* **52**(3), 449-455 (2013).
2.A. N. Miliou, R. Srivastava, R. V. Ramaswamy. "A 1.3-μm directional coupler polarization splitter by ion exchange," *J. Lightw. Technol.* **11**(2), 220-225 (1993).
3.G. D. Peng, T. Tjugiarto, P. L. Chu. "Polarisation beam splitting using twin-elliptic-core optical fibres," *Electron. Lett.* **26**(10), 682-683 (1990).
4.C. W. Wu, T. L. Wu, H. C. Chang. "A novel fabrication method for all-fiber, weakly fused, polarization beamsplitters," *IEEE Photon. Technol. Lett.* **7**(7), 786-788 (1995).
5.T. A. Birks, J. C. Knight, P. S. J. Russell. "Endlessly single-mode photonic crystal fiber," *Opt. Lett.* **22**(13), 961-963 (1997).
6.J. C. Knight, T. A. Birks, R. F. Cregan, et al. "Large mode area photonic crystal fibre," *Electron. Lett.* **34**(13), 1347-1348 (1998).
7.A. Ortigosa-Blanch, J. C. Knight, W. J. Wadsworth, et al. "Highly birefringent photonic crystal fibers," *Opt. Lett.* **25**(18), 1325-1327 (2000).
8.M. J. Steel, R. M. Osgood. "Polarization and dispersive properties of elliptical-hole photonic crystal fibers," *J. Lightw. Technol.* **19**(4), 495 (2001).
9.T. P. Hansen, J. Broeng, S. E. B. Libori, et al. "Highly birefringent index-guiding photonic crystal fibers," *IEEE Photon. Technol. Lett.* **13**(6), 588-590 (2001).
10.Q. Liu, S. G. Li, Z. K. Fan, et al. "Numerical analysis of ultrabroadband polarization splitter based on gold-filled dual-core photonic crystal fiber," *Opt. Commun.* **334**, 46-50 (2015).
11.S. Kim, C. S. Kee. "Dispersion properties of dual-core photonic-quasicrystal fiber," *Opt. Express* **17**(18), 15885-15890 (2009).
12.X. Li, Z. Xu, W. Ling, et al. "Design of highly nonlinear photonic crystal fibers with flattened chromatic dispersion," *Appl. Opt.* **53**(29), 6682-6687 (2014).
13.L. Zhang, C. Yang. "Polarization splitter based on photonic crystal fibers," *Opt. Express* **11**(9), 1015-1020 (2003).
14.M. F. O. Hameed, S. S. A. Obayya. "Polarization splitter based on soft glass nematic liquid crystal photonic crystal fiber," *IEEE Photon. J.* **1**(6), 265-276 (2009).
15.M. Y. Chen, B. Sun, Y. K. Zhang, et al. "Design of broadband polarization splitter based on partial coupling in square-lattice photonic-crystal fiber," *Appl. Opt.* **49**(16), 3042-3048 (2010).
16.L. Jiang, Y. Zheng, L. Hou, et al. "An ultrabraoadband polarization splitter based on square-lattice dual-core photonic crystal fiber with a gold wires," *Opt. Commun.* **351,** 50-56 (2015).

17. C. Dou, X. Jing, S. Li, et al. "A compact and low-loss polarization splitter based on dual-core photonic crystal fiber," *Opt. Quant. Electron.* **50**(6), 255 (2018).
18. X. Wang, S. Li, H. Chen, et al. "Polarization splitter based on dual-core photonic crystal fiber with octagonal lattice," *Opt. Quant. Electron.* **48**(4), 271 (2016).
19. N. Florous, K. Saitoh, M. Koshiba. "A novel approach for designing photonic crystal fiber splitters with polarization-independent propagation characteristics," *Opt. Express* **13**(19), 7365-7373 (2005).
20. D. Rajeswari, A. S. Raja, S. Selvendran. "Design and analysis of polarization splitter based on dual-core photonic crystal fiber," *Optik.* **144**, 15-21 (2017).
21. F. He, W. Shi, Z. Hui, et al. A dual-core PCF polarization splitter with five elliptical air holes based on tellurite glass," *Opt. Quant. Electron.* **49**(11), 363 (2017).
22. Z. Xu, X. Li, W. Ling, et al. "Design of short polarization splitter based on dual-core photonic crystal fiber with ultra-high extinction ratio," *Opt. Commun.* **354**, 314-320 (2015).
23. E. L. Wang, H. M. Jiang, K. Xie, et al. "Polarization splitter based on dual core liquid crystal-filled holey fiber," *J. Appl. Phys.* **120**(11), 114501 (2016).
24. H. Wang, X. Yan, S. Li, et al. "Tunable surface plasmon resonance polarization beam splitter based on dual-core photonic crystal fiber with magnetic fluid," *Opt. Quant. Electron.* **49**(11), 368 (2017).
25. J. S. Wang, L. Pei, S. J. Weng, et al. "Ultrashort polarization beam splitter based on liquid-filled dual-core photonic crystal fiber," *Appl. Opt.* **57**(14), 3847-3852 (2018).
26. Q. Xu, W. L. Luo, K. Li, et al. "Design of polarization splitter via liquid and Ti infiltrated photonic crystal fiber," *Crystals* **9**(2), 103 (2019).
27. Y. W. Qu, J. H. Yuan, X. Zhou, et al. "Surface plasmon resonance-based silicon dual-core photonic crystal fiber polarization beam splitter at the mid-infrared spectral region," *J. Opt. Soc. Am. B* **37**(8), 2221-2230 (2020).
28. Q. Liu, L. Xing, Z. X. Wu, et al. "High-sensitivity photonic crystal fiber force sensor based on Sagnac interferometer for weighing," Opt. Laser Technol. **123**, 105939 (2020).
29. I. H. Malitson, "Interspecimen comparison of the refractive index of fused silica," *J. Opt. Soc. Am. A* **55**(10), 1205-1209 (1965).
30. J. W. Fleming, "Dispersion in GeO2 -SiO2 glasses," *Appl. Opt.* **23**(24), 4486-4493 (1986).
31. A. Vial, A. S. Grimault, Macías D, et al. "Improved analytical fit of gold dispersion: Application to the modeling of extinction spectra with a finite-difference time-domain method," *Phys. Rev. B* **71**(8), 085416 (2005).
32. K. Saitoh, Y. Sato, M. Koshiba, "Coupling characteristics of dual-core photonic crystal fiber couplers," *Opt. Express* **11**(24), 3188-3195 (2003).
33. M. Eisenmann, E. Weidel, "Single-mode fused biconical coupler optimized for polarization beamsplitting," *J. Lightw. Technol.* **9**(7), 853-858 (1991).
34. N. Florous, K Saitoh, M. Koshiba, "A novel approach for designing photonic crystal fiber splitters with polarization-independent propagation characteristics," *Opt. Express* **13**(19), 7365-7373 (2005).
35. Z. H. Zhang, Y. F. Shi, B. M. Bian, et al. "Dependence of leaky mode coupling on loss in photonic crystal fiber with hybrid cladding," *Opt. Express* **16**(3), 1915-1922 (2008).
36. A. Khaleque, E. G. Mironov, H. T. Hattori, "Analysis of the properties of a dual-core plasmonic photonic crystal fiber polarization splitter," *Appl. Phys. B* **121**(4), 523-532 (2015).
37. N. Gómez-Cardona, C. Jiménez-Durango, J. Usuga-Restrepo, et al. "Thermo-optically tunable polarization beam splitter based on selectively gold-filled dual-core photonic crystal fiber with integrated electrodes," *Opt. Quant. Electronics.* **53**(2), 1-15 (2021).
38. L. Chen, W. Zhang, Z. Zhang, et al. "Design for a single-polarization photonic crystal fiber wavelength splitter based on hybrid-surface plasmon resonance," *IEEE Photon J.* **6**(4), 1-9 (2014).
39. N. Chen, X. Zhang, X. Lu, et al. "Numerical investigation of a short polarization beam splitter based on dual-core photonic crystal fiber with As2S3 layer," *Micromachines.* **11**(7), 706 (2020).
40. Z. K. Fan, S. G. Li, Y. Q. Fan, et al. "Designing analysis of the polarization beam splitter in two communication bands based on a gold-filled dual-core photonic crystal fiber," *Chin. Phys. B.* **23**(9), 094212 (2014).

41. C. Jimenez-Durango, E. Reyes-Vera, N. Gomez-Cardona, "Ultra-short polarization beam splitter to operate in two communication bands based on a gold-filled dual-core photonic crystal fiber," *J. Appl. Phys.* **Tu4A**, 16 (2018).
42. A. Khaleque, H. T. Hattori, "Ultra-broadband and compact polarization splitter based on gold filled dual-core photonic crystal fiber," *J. Appl. Phys.* **118**(14), 143101 (2015).

Ke Wang is currently a graduate student in the state Key Laboratory of Information Photonics and Optical Communication department at Beijing University of Posts and Telecommunications.

Yuwei Qu is currently working toward the Ph.D. degree in electronic science and technology at Beijing University of Posts and Telecommunications (BUPT), Beijing, China. His research interests include photonic crystal fiber, surface plasmon reasonance, and novel fiber devices.

Jinhui Yuan received the Ph.D. degree in physical electronics from Beijing University of Posts and Telecommunications (BUPT), Beijing, China, in 2011. He is currently a Professor at the Department of computer and communication engineering, University of Science and Technology Beijing (USTB). His current research interests include photonic crystal fibers, silicon waveguide, and optical fiber devices. He is the Senior Members of the IEEE and OSA.

Shi Qiu is currently working toward the Ph.D. degree in electronic science and technology at Beijing University of Posts and Telecommunications (BUPT), Beijing, China. His research interests include photonic crystal fiber sensors.

Xian Zhou received the Ph.D. degree in electromagnetic field and microwave technology from Beijing University of Posts & Telecommunications (BUPT), Beijing, China, in 2011. She is currently an Professor at the Department of Computer and Communication Engineering, University of Science & Technology Beijing (USTB). Her research interests are focused on highspeed optical communications, short reach communications, and digital signal nprocessing.

Binbin Yan received the B.S. and M.S. degrees from Beijing University of Posts and Telecommunications (BUPT), Beijing, China, in 2003 and 2005, respectively. In 2009, she received the Ph.D. degree from BUPT. Now she is with the BUPT as an Associate Professor. Her research interests include photonic devices and fiber optic sensing.

Qiang Wu received the B.S. and Ph.D. degrees from Beijing Normal University and Beijing University of Posts and Telecommunications, Beijing, China, in 1996 and 2004, respectively. From 2004 to 2006, he worked as a Senior Research Associate in City University of Hong Kong. From 2006 to 2008, he took up a Research Associate post in Heriot-Watt University, U.K. From 2008 to 2014, he worked as a Stokes Lecturer at Photonics Research Centre, Dublin Institute of Technology, Ireland. He is currently an Associate Professor at Northumbria University, U.K. His research interests include photonics devices and fiber optic sensing.

Bin Liu received his B.S. and Ph.D. degree from Sun Yat-sen University, China. Dr. Liu is an associate Professor with Key Laboratory of Opto-Electronic Information Science and Technology of Jiangxi Province, Nanchang Hangkong University, Nanchang 330063, China. His research interests include optical fiber sensing and signal processing, nanofiber, microsphere sensors for bio-chemical sensing, nonlinear fiber optics, surface plasmon resonant.

Kuiru Wang received the B.S. and M.S. degrees from Beijing University of Posts and Telecommunications (BUPT), Beijing, China, in 1984 and 1990, respectively. In 2009, she received the Ph.D. degree from BUPT. Now she is with the BUPT as a Professor. Her current research interests include optical fiber communication and photonic devices.

Xinzhu Sang received the Ph.D. degree from Beijing University of Posts and Telecommunications (BUPT), Beijing, China, in 2005. Now he is with the BUPT as a professor. His current research interests include novel photonic devices, optical communication and optical interconnect. Prof. Sang is a senior Member of Chinese Institute of Communication, a committee of Holography and Optical information Processing, Chinese Optical Society, and a member of OSA.

Chongxiu Yu graduated from the Beijing University of Posts and Telecommunications (BUPT), Beijing, China, in 1969. Now she is with the BUPT as a Professor. Up to now she has published more than 300 papers. Her Research interests are the optical fiber communication, photonic switching, and optoelectronics technology and its applications. Prof. Yu is the Members of Chinese Institute of Communication, Committee of Fiber Optics and Integral Optics, and Chinese Optical Society.

Captions List

Fig. 1. The cross-section of the proposed DC-PCF PBS.

Fig. 2. The effective refractive indices of the *x*-pol odd and even modes, *y*-pol odd and even modes, *x*-pol and *y*-pol first SPP modes, and zero SPP mode calculated as functions of wavelength.

Fig. 3. The mode field distributions of the *x*-pol odd mode, *x*-pol even mode, *y*-pol odd mode, and *y*-pol even mode calculated at wavelengths (a) 1.05 μm and (b) 1.55 μm.

Fig. 4. The relationships between the *CLx*, *CLy*, and *CLR* and *d*.

Fig. 5. The relationships between the *CLx*, *CLy*, and *CLR* and (a) Λ_1 and (b) Λ_2.

Fig. 6. The relationships between the *CLx*, *CLy*, and *CLR* and (a) d_{x1} and (b) d_{y1}.

Fig. 7. The relationships between the *CLx*, *CLy*, and *CLR* and (a) dx_2 and (b) dy_2.

Fig. 8. The relationships between the *CLx*, *CLy*, and *CLR* and (a) dx_3 and (b) dy_3.

Fig. 9. The relationships between the *CL* and *CLR* and wavelength, (a) without gold wires, and (b) with gold wires.

Fig. 10. The relationship between P_{out} of the *x*-pol and *y*-pol and propagation distance, and (b) the relationship between the *ER* and wavelength.

Fig. 11. The relationships between the *ER* and wavelength under ±1% error of (a) *d*, (b) dx_1, dy_1 (c) dx_2, dy_2, and (d) dx_3, dy_3.

Table 1. The comparisons between other proposed PCF PBS and this work.